Interplay between Smectic Ordering and Microphase Separation in a Series of Side-Group Liquid-Crystal Block Copolymers

ARTICLE *in* MACROMOLECULES · JUNE 2004

Impact Factor: 5.8 · DOI: 10.1021/ma0498619 · Source: OAI

Interplay between Smectic Ordering and Microphase Separation in a Series of Side-Group Liquid-Crystal Block Copolymers

I. W. Hamley* and V. Castelletto

Department of Chemistry, University of Leeds, Leeds LS2 9JT, UK

Z. B. Lu, C. T. Imrie, and T. Itoh†

Department of Chemistry, University of Aberdeen, Meston Walk, Old Aberdeen AB24 3UE, UK

M. Al-Hussein

FOM-Institute for Atomic and Molecular Physics, Kruislaan 407, 1098 SJ, Amsterdam, The Netherlands

Received January 20, 2004; Revised Manuscript Received March 23, 2004

ABSTRACT: Hierarchical ordering in a series of side-group liquid-crystal block copolymers was investigated in the bulk via differential scanning calorimetry (DSC), polarized light microscopy, small-angle X-ray scattering (SAXS), and small-angle neutron scattering (SANS). The diblock copolymers comprise a polystyrene block and a block of poly(methyl methacrylate) bearing a chiral biphenyl ester mesogenic unit linked to the backbone by a dodecyloxy spacer. A series of copolymers with different volume fractions of mesogenic block were prepared by atom transfer radical polymerization. Ordering of mesogens into a smectic phase is characterized by a period 3.5 nm. Glass transition temperatures and the clearing temperature for each sample were determined by DSC. Additional ordering occurs due to microphase separation of the block copolymer at a length scale of 22−27 nm, as confirmed by SAXS and SANS. The order−disorder transition was found to be coincident with the smectic−isotropic transition for a sample comprising PS cylinders. A hexagonal morphology was determined for samples with both a minority and a majority liquid-crystal block. Remarkably, the morphology comprising liquid-crystal (LC) cylinders in a polystyrene matrix could be oriented by slow cooling through the clearing temperature, in the presence of a strong magnetic field. The inverse morphology of cylinders formed by the PS block in an LC matrix was not oriented in this way. This is ascribed to the nucleation of defects around the nanorods in the LC matrix. The thin film nanostructure was investigated by atomic force microscopy (AFM) and X-ray reflectivity for a sample comprising PS cylinders. AFM confirmed a hexagonal-packed cylinder morphology in thin films with coexisting parallel and perpendicular orientations of rods with respect to the substrate. The presence of Bragg peaks in specular X-ray reflectivity intensity profiles indicates a proportion of smectic layers lying parallel to the substrate, with a spacing similar to that in bulk. Our results provide a comprehensive picture of hierarchical ordering in the bulk and in thin films.

1. Introduction

Side-group liquid-crystal polymers (SGLCPs) have considerable application potential in a range of advanced electrooptic technologies.[1,2] At the root of this potential is the unique duality of properties exhibited by SGLCPs: specifically, a combination of macromolecular characteristics such as mechanical integrity and ease of processability, with the electrooptic properties, albeit on a much slower time scale, of low molar mass liquid crystals.[1]

Block copolymers, on the other hand, have attracted attention because it is possible to tailor the properties in a kind of polymeric "alloy" by combining blocks with distinct characteristics (glassy, rubbery, crystalline). In addition, they form a range of microphase-separated structures. For diblock copolymers these are lamellae, hexagonal-packed cylinders, cubic-packed spheres, and a bicontinuous cubic gyroid morphology.[3]

The coupling of a mesogenic block to an isotropic block in a side-group liquid-crystal block copolymer (SGLC-BCP) leads to the interplay between liquid crystallinity and microphase separation of the block copolymer. The mesogen influences the microphase structure of the block copolymer and vice versa. It has been reported that the region of stability of the lamellar phase is enhanced in certain SGLC-BCPs compared to coil−coil diblocks,[4] but not in others,[5] although it may be shifted in composition range.[4,6] The origin of these changes in phase stability is the change in interfacial curvature, resulting from the elastic properties of the liquid-crystalline block. A free energy model has been developed to account for this that considers the interaction of mesogens, the stretching of the amorphous chains, and the elastic deformation of the backbone due to the liquid-crystalline ordering.[7] The strength of segregation of the two blocks in a side-group liquid-crystal block copolymer is larger than for most coil−coil diblocks, as parametrized by a larger Flory−Huggins interaction parameter. The microphase separation also influences the conformation of the liquid-crystalline block and the orientational ordering of the mesogens. The conformation of the liquid-crystalline block is constrained by the coupling of this block to the isotropic block.[8] This is similar to the situation in amorphous−crystalline block copolymers, where the folding of the crystalline block is influenced by the amorphous block.[9] Equilibrium chain folding can occur (in contrast to homopolymers)

† Permanent address: Department of Applied Chemistry, Ehime University, 3 Bunkyo-cho, Matsuyama-shi, Ehime 790-8577, Japan.

* To whom correspondence should be addressed.

10.1021/ma0498619 CCC: $27.50
Published on Web 05/29/2004

due to the requirement to balance the interfacial area of both blocks. At the same time, the conformation of the amorphous block (isotropic block for SGLC-BCPs) is influenced.

Flow alignment has enabled examination of the orientation of mesogens with respect to the microstructure.[4,5,10−12] It will depend on the composition of the copolymer (which in turn controls the microphase symmetry) and on the size of the microphase-separated domains (finite size effect).[8] If the liquid crystal is confined within spheres, smectic phase formation is suppressed, and instead a nematic phase has been observed.[5,10] In contrast, when the liquid-crystalline domain is continuous, smectic phases can form. Considering, for example, lamellar phases, the smectic layers are usually aligned perpendicular to the block copolymer lamellae.[5,8,11,13,14] However, a parallel alignment has been reported for a smectic C*-forming mesogen.[15] It was proposed that the distinct orientation resulted from a decoupling of mesogenic order from that of the block copolymer due to the longer spacer attaching the mesogen to the backbone. For samples forming liquid-crystalline cylinders, a homogeneous orientation of mesogens parallel to the walls of the cylinders has been reported.[11,16] For the inverse structure (continuous liquid-crystalline phase) smectic layers have been found to lie parallel to the cylinders[5,17] or tilted with respect to them.[4]

Liquid-crystal phase transition temperatures are usually found to be similar to those of the corresponding homopolymers (although the transition enthalpy may differ).[8] However, Zheng and Hammond report a stabilization of the smectic phase by the lamellar block copolymer microstructure.[18] Liquid-crystalline phase transitions also influence the microphase structure. For example, the isotropic−nematic transition for one polymer was observed to induce a transition in the microphase-separated morphology (from body-centered-cubic spheres to cylinders).[19] In another case, a transition from a mixed lamellar/cylinder morphology to a pure lamellar morphology was induced by the change in interfacial curvature resulting from the loss of liquid-crystalline ordering.[20] Work by the same group indicates an order−order transition from disks to spheres of polystyrene driven by the liquid-crystal clearing transition.[6]

Hierarchical ordering in side-group liquid-crystal block polymers can be compared to that observed in diblocks in which amphiphilic molecules are attached via hydrogen bonds to one block. In particular, Ikkala et al. have investigated a diblock system with amphiphilic molecules attached via hydrogen bonds to one block. In particular, they investigated hierarchical order in polystyrene−poly(4-vinylpyridine) (PS−P4VP) diblocks with pentadecylphenol side chains attached via hydrogen bonding to the P4VP block.[21,22] Although the hydrogen bond is much weaker than a covalent bond, the side-chain length is similar in their system and in our side-group liquid-crystal block copolymer.

Here, we report the characterization of hierarchical order in the bulk and in thin films of side-chain liquid-crystalline block copolymers with structures

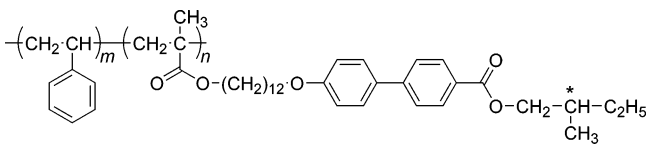

Scheme 1. Synthesis of Diblock Liquid-Crystalline Copolymers

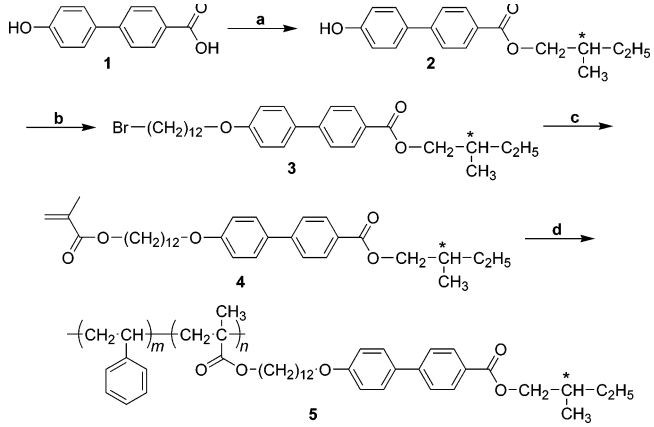

The mesogen is chiral and expected to favor formation of a smectic C* structure. The composition (ratio of *m* and *n*) was varied in a series of 10 synthesized block copolymers. Simultaneous small-angle X-ray scattering (SAXS) and wide-angle X-ray scattering (WAXS) provide evidence for hierarchical ordering in the bulk: microphase separation between the two blocks, together with smectic ordering of the mesogens. Alignment in a magnetic field was studied using small-angle neutron scattering (SANS) on polymers in which the polystyrene block was selectively deuterated to provide contrast. The bulk phase behavior is compared to that in thin films, which was probed using atomic force microscopy (AFM) and X-ray reflectivity. The former technique directly images the structure at the surface, whereas the latter provides information on the order perpendicular to the surface. In a previous note, we presented preliminary results on hierarchical order and shear-induced order in one of the copolymers in the present series.[23]

2. Experimental Section

2.1. Synthesis. Polymers were prepared via atom transfer radical block copolymerization of styrene with (*S*)-(−)-methylbutyl 4′-(12-methacryloyloxydodecyloxy)biphenyl-4-carboxylate. Scheme 1 summarizes the synthesis. The following details for sample Z11 are representative for the other polymers synthesized (Table 1).

Reagents and Conditions. Styrene and deuterated styrene (*d*8) were purified by standard methods and distilled over calcium hydride. All other reagents were used as received.

a. (*S*)-(−)-Methylbutanol, toluene, 0.5 mL sulfuric acid, reflux, 3 days. b. 1,12-Dibromododecane, potassium carbonate, acetone, 2 days. c. Methacrylic acid, potassium hydrocarbonate, dimethylformide, 100 °C, overnight. d. PS−Br, spartein, copper bromide, anisole, 90 °C.

The chiral monomer **4** was prepared according to a procedure to be detailed elsewhere.[24] The homopolymer and diblock copolymers were prepared by the method of atom transfer radical polymerization (Scheme 1), and the unreacted prepolymer PS−Br could be easily removed by Soxhlet extraction using methylcyclohexane, which gave pure diblock copolymer. In the case of deuterated diblock copolymer, fully deuterated styrene was used to prepare the prepolymer *d*PS−Br.

Polymerization. To a polymerization ampule, copper bromide (16.3 mg) was first added; then the solution of PS−Br (1460.0 mg, $M_n = 1.31 \times 10^4$, $M_w/M_n = 1.16$), (*S*)−(−)-methylbutyl 4′-(12-methacryloyloxydodecyloxy)biphenyl-4-carboxylate (541.2 mg, 1.01 mmol), and spartein (52.7 mg, 0.225 mmol) in anisole (1185.6 mg) was added. The ampule was connected to a high-vacuum system, degassed at liquid nitrogen temperature three times, and sealed under high vacuum. The polymerization was carried out at 90 °C for 40 min. The polymerization mixture

Table 1. Conditions of Block Copolymerization with PS-Br by ATRP[a]

name	[**4**]/wt %	[PS-Br][b]/wt %	[CuBr]/wt %	[Spartein]/wt %	concn[c] (wt %)	time[d] (min)	conv[e] (%)
Z01	21	1	1.0	2.02	33	60	
Z04	22	1	1.0	2.02	33	40	
Z09	47	1	1.1	2.04	33	40	
Z10	24	1	1.2	2.09	33	40	
Z11	9.1	1	1.0	2.03	17	90	
Z12	20	1	1.3	2.06	20	450	60
Z13	13	1	0.98	1.97	15	450	65
Z14	10	1	1.0	2.53	12	450	64
Z22d[f,g]	54	1	1.2	2.00	25	360	37
Z23d[f]	51	1	1.1	2.09	25	390	81

[a] ATRP carried out at 90 °C. [b] Using PS-Br as initiator. [c] Concentration of LC monomer. [d] Reaction time. [e] Polymerization conversion determined by ^{1}H NMR. [f] Using *d*PS-Br as initiator. [g] Four methylene units of spacer in SGLCP segment.

was first passed through a short column of aluminum oxide (activated, basic, Brockmann I), with tetrahydrofuran as eluent to remove copper slats. The solution was concentrated and precipitated into a large amount of methanol. The crude product was collected, Soxhlet extracted using methanol overnight (to remove unreacted monomer), then Soxhlet extracted using methylcyclohexane overnight (to remove unreacted polystyrene), extracted with dichloromethane, concentrated, and reprecipitated into methanol. The removal of the monomer from the polymer was confirmed by the disappearance of the peaks associated with the alkene protons at 5.8 and 6.1 ppm in the ^{1}H NMR spectra of the monomer. The removal of unreacted polystyrene was confirmed by GPC. Yield 0.5 g.

2.2. Characterization. ^{1}H NMR spectra were measured in $CDCl_3$ on a Bruker AC-F 250 MHz NMR spectrometer. The molecular weights of the polymers were measured by gel permeation chromatography using a Knauer Instruments chromatograph equipped with two PL gel 10 μm mixed columns and controlled by Polymer Laboratories GPC SEC V5.1 software. Chloroform was used as the eluent. A calibration curve was obtained using polystyrene standards.

2.3. Differential Scanning Calorimetry. The thermal properties of the polymers were determined by differential scanning calorimetry (DSC) using a Metter-Toledo 821 DSC equipped with an autocool accessory and calibrated using indium and zinc standards. Two aliquots were used for each polymer and the results averaged. The heating and cooling rate in all cases was 10 °C min^{-1}. Phase identification was performed by polarized light microscopy using an Olympus BH-2 optical microscope equipped with a Linkam THMS 600 heating stage and TMS 91 control unit.

2.4. SAXS and WAXS. SAXS experiments were performed at the Synchrotron Radiation Source (SRS) at Daresbury Laboratory, Warrington, UK. Samples were studied both at rest and during shear. (The latter experiments were performed separately.) The static experiments were performed on beamlines 2.1 and 16.1. Experiments on the sample under shear were performed on station 16.1. On station 2.1, the sample-to-detector distance was 3.25 m, and the wavelength was $\lambda =$ 1.5 Å. A gas-filled area detector was used to collect data. On station 16.1, camera lengths of 1.3, 2.0, and 6.0 m were used. The wavelength was $\lambda = 1.41$ Å. WAXS data were also acquired during static measurements on station 16.1. Quadrant SAXS data were used for measurements on the unsheared sample, with a curved linear multiwire WAXS detector. For the measurements under shear, the RAPID two-dimensional SAXS detector was used.

For static measurements, the sample in thin film form was mounted in a TA Instruments DSC pan fitted with mica windows to allow transmission of the X-ray beam. The loaded pans were placed in the cell of a Linkam DSC of single-pan design. The experiments were carried out for temperatures ranging between 25 and 125 °C. For the shear experiments, the sample was subjected to oscillatory shear at 95 °C using a modified Rheometrics RSA II rheometer. The sample was mounted as a film in a shear sandwich geometry; i.e., two films were placed between fixed outer plates and a central oscillating inner plate. The shear direction was vertical, and the X-ray beam was incident along the shear gradient direction. Further details of this instrument are provided elsewhere.[25] For all SAXS measurements, scattering patterns from wet collagen (rat-tail tendon) were used for calibration of the q scale ($|q| = 4\pi \sin\theta/\lambda$, where the scattering angle is 2θ), and corrections for detector response were made. The data collected using two-dimensional area detectors were reduced to one-dimensional form by sector averaging.

2.5. Small-Angle Neutron Scattering. SANS experiments were conducted on beamline D22 at the Institut Laue-Langevin (ILL), Grenoble, France, and on LOQ at ISIS, Rutherford Appleton Laboratory, UK. On D22, samples were placed within a spacer ring between quartz plates. This sample cell was placed into an electrically heated rack for automated positioning in the neutron beam. The wavelength was $\lambda = 6$ Å. Sample-to-detector distances of 11.2 and 1.8 m were used to cover small-angle and wide-angle regions, respectively. The q range ($q = 4\pi \sin\theta/\lambda$, where 2θ is the scattering angle) covered was $q = 0.0042-0.49$ Å^{-1}, with an overlap between the two q ranges in the intermediate region. On LOQ, the quartz disk sample assembly was mounted in an electromagnet, with electrical heat control which was monitored via thermocouples. A magnetic field, estimated at 1.8 T, was applied to the sample, starting in the isotropic melt and slowly cooling (just under 4 °C/h) to 70 °C, i.e., through the smectic phase and then below the polystyrene glass transition temperature. LOQ is a time-of-flight instrument, and wavelengths in the range $2.2 < q/$Å$^{-1} < 10$ were used in converting to a q scale. The q range covered was $0.006-0.24$ Å^{-1} on the main detector. The wide-angle detector bank was not used since most wide-angle scattering was blocked by the electromagnet arms.

2.6. Atomic Force Microscopy. Samples were spin-coated from 2% polymer solution onto Si wafers and annealed overnight at 130 °C. Tapping mode AFM (Nanoscope III, Digital Instrument) was used to image the polymer surface. The AFM was operated under ambient conditions with commercial silicon microcantilever probe tips. The manufacturer's values for the probe tip radius and force constant are <10 nm and in the range of $31-71$ N m^{-1}, respectively. Topographic and phase images were obtained simultaneously using a resonance frequency of approximately 165 kHz for the probe oscillation.

2.7. X-ray Reflectivity. X-ray reflectivity measurements were performed using a rotating copper anode (Rigaku RU-300H) generator fitted with a two-circle diffractometer. The generator was operated at a maximum power of 18 kW. A copper Kα_1 radiation beam (wavelength $\lambda = 0.154$ nm) was collimated by a parabolic graded multilayer mirror and a presample slit of (0.1×6) mm^2. All samples were investigated under specular reflection conditions at several temperatures after equilibration for about 12 h. The specular reflectivity of X-rays provides information on the electron density variation normal to the surface, averaged over the footprint of the incident beam. The scattering vector q in specular reflectivity is defined by $q = 4\pi \sin\theta/\lambda$, where θ is the incident or reflective angle with respect to the horizontal plane and λ is the wavelength of the incident X-rays. All measurements were

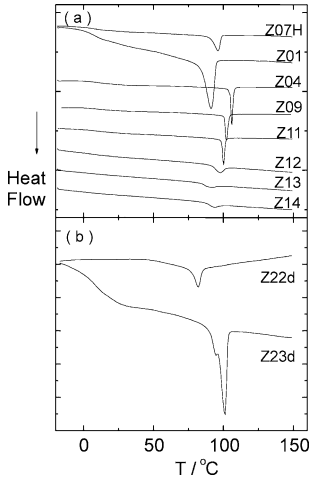

Figure 1. DSC curves for (a) homopolymer and block copolymers and (b) deuterated block copolymers. In each part, DSC curves are shown on a common scale. Parts a and b are not on the same scale.

performed in the range $\theta = 0.00°-2.40°$ with a 0.01° step. The corresponding q range was from $q = 0.00-0.29$ Å^{-1}.

3. Results and Discussion

3.1. Thermal Properties. Differential scanning calorimetry was used to locate phase transitions and to determine the enthalpy associated with the smectic−isotropic transition. Normalized DSC data are presented in Figure 1. The enthalpy change, ΔH, for the smectic−isotropic transition was calculated as follows:

$$\Delta H\ (\text{kcal mol}^{-1}) = \frac{\Delta H_{\text{meas}}\ (\text{J g}^{-1})\ M\ (\text{g mol}^{-1})}{4.184 \times 10^3\ (\text{J kcal}^{-1}) w_{\text{LC}}}$$

Here, M is the monomer molar mass (g mol^{-1}) and w_{LC} is the weight fraction of LC block.

Data for a homopolymer of the liquid-crystal block are included in Figure 1a for comparison with the nondeuterated block copolymers. In the block copolymers, the clearing point coincides closely with a transition ascribed to the glass transition of the PS block, which occurs close to 100 °C, depending somewhat on molar mass. An additional inflection point centered on approximately 5 °C is assigned to the glass transition temperature of the mesogen-bearing block. This transition is clearly seen for the mesogenic homopolymer (Figure 1a, Table 3). For the block copolymers, no obvious trend in clearing temperature is apparent as a function of either molar mass or copolymer composition. However, the normalized enthalpy at the clearing point is, as expected, much lower for the three samples (Z12, Z13, and Z14) that contain a minority of LC block. This behavior is also observed when the two deuterated polymers are considered (Figure 1b). The glass transition temperatures of both blocks are very well resolved for sample Z23d, with a majority of LC block. In particular, the glass transition of polystyrene is separated from the smectic−isotropic transition (at 101.8 °C). The clearing point temperatures and associated enthalpies are listed in Table 3.

3.2. Bulk Nanostructures. Wide-angle X-ray scattering was used to confirm smectic layer structures. All diblock copolymers listed in Table 2 (except Z22d and Z23d where it has not been confirmed) showed a smectic layer peak at $d = 35 \pm 0.5$ Å. This is identical to that observed for the two homopolymers Z07 and Z08 (data not shown) and corresponds to the length of the mesogens (including spacer) calculated from a molecular model (ACDlabs Freeview 5.0). For selected samples, experiments were performed where wider angles (larger q) were accessed. Typical data (in this case for sample Z12) are shown in Figure 2. This shows two orders of equally spaced reflections, confirming a smectic structure.

Table 2. DSC and NMR Characterization of Block Copolymers and Homopolymers[a]

name	$M_{n,total}$[b]	M_w/M_n[b]	$M_{n,PS-Br}$[b,c]	M_w/M_n[b,c]	Φ_{LC}[d]
Z01	31 200	1.32	5 900	1.13	0.81
Z04	25 600	1.22	5 900	1.13	0.77
Z07H	22 000	1.16			1
Z08H	25 000	1.21			1
Z09	41 600	1.19	13 000	1.15	0.70
Z10	27 200	1.20	13 400	1.16	0.50
Z11	33 900	1.16	13 100	1.14	0.60
Z12	17 700	1.44	18 800	1.28	0.34
Z13	16 100	1.37	15 700	1.27	0.20
Z14	19 700	1.34	19 400	1.25	0.16
Z22d[f,g]	12 356	1.46	8 429	1.34	0.32
Z23d[f]	28 665	1.67	8 429	1.34	0.71

[a] Homopolymers are denoted with a suffix H. Polymers with a deuterated polystyrene block are denoted with a suffix d. All syntheses were carried out at 90 °C. [b] Molecular weight and molecular weight distribution determined by GPC calibrated with polystyrene standard. [c] Molecular weight of polystyrene precursor synthesized by ATRP. [d] Weight fraction of side-chain liquid-crystalline polymer segment determined by ^{1}H NMR. [f] Using dPS-Br as initiator. [g] Four methylene units of spacer in SGLCP segment.

Table 3. DSC Characterization of Block Copolymers[a]

	T_i/°C[b] (ΔH/kcal mol^{-1} [c])		
sample	heating	cooling	T_g/°C[d]
Z01	96.1 (1.10)	92.1 (1.05)	
Z04	91.2 (1.02)	87.6 (1.03)	
Z07H	95.1(1.18)	90.2 (1.06)	7
Z08H	93.4 (1.24)	91.9 (1.08)	6
Z09	106.1 (1.09)	100.6 (1.16)	
Z10	100.2 (1.24)	96.5 (1.08)	
Z11	102.2 (1.01)	97.5 (1.05)	around 5
Z12	97.6 (1.33)	95.1 (1.11)	
Z13	90.4 (1.71)	85.4 (0.99)	
Z14	93.7 (1.80)	88.3 (1.06)	
Z22d	83.0	75	
Z23d	101.8	98.3	18

[a] Determined by DSC measurement on second heating and cooling at the rate of 10°C min^{-1}. [b] Transition temperature. [c] Corresponding enthalpy change estimated per mole of the side-chain liquid-crystalline polymer (SGLCP) segment. [d] Glass transition temperature of the SGLCP segment.

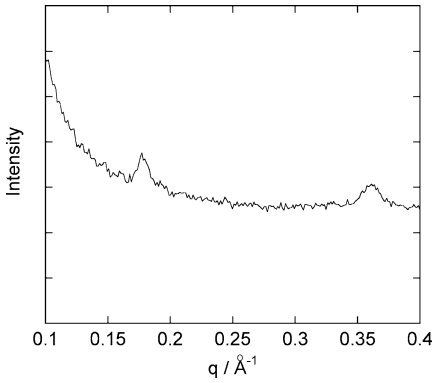

Figure 2. WAXS data for sample Z12 at 30 °C.

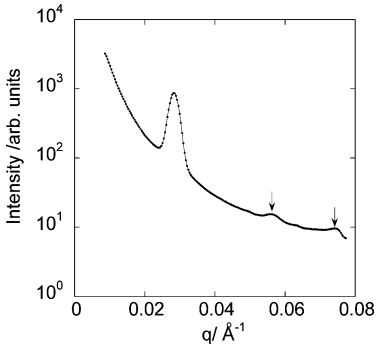

Figure 3. SAXS data for Z11 obtained after cooling from liquid crystal phase to 25 °C.

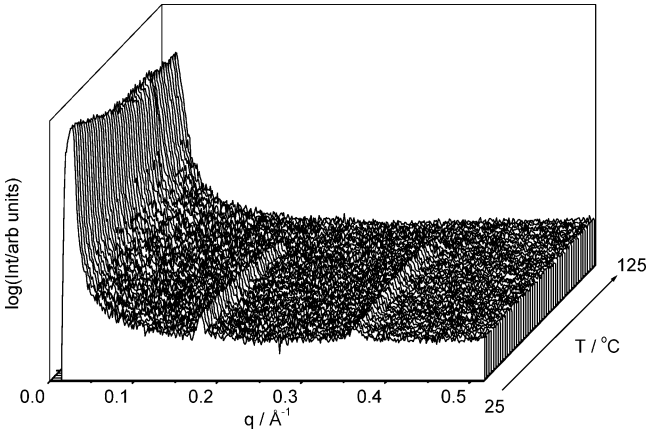

Figure 4. WAXS data for Z11 obtained during a heating ramp from 25 to 125 °C at 5 °C/min.

Table 4. SAXS Data

sample	morphology (temp range)	q^*/Å^{-1} (±0.0005)
Z01	no small-angle peaks	
Z04	no small-angle peaks	
Z09	not determined	0.0280
Z10	no small-angle peaks	
Z11	hexagonal	0.0285
Z12	no small-angle peaks	
Z13	no small-angle peaks	
Z14	no small-angle peaks	
Z22d	hexagonal	0.023 (±0.001, SANS)
Z23d	hexagonal	0.023 (±0.001, SANS)

Evidence for microphase-separated structures was obtained for many samples. Although in several cases, the morphology could not be confirmed since only a single Bragg reflection was obtained in other cases the presence of higher order reflections facilitated phase identification. Where it could be determined, the morphology is listed in Table 4. As an example, SAXS provides evidence for a hierarchically ordered structure formed by self-assembly in Z11. Figure 3 shows SAXS data obtained after cooling from the liquid crystal phase to 25 °C. A sharp peak from a microphase-separated structure is evident at $q^* = 0.0285 \pm 0.0005$ Å^{-1} and corresponds to a structural period $d_m = 220 \pm 4$ Å. Weak higher order peaks at $2q^*$ and $\sqrt{7}q^*$ indicate that the morphology is hexagonal-packed cylinders. (In separate experiments a $\sqrt{3}q^*$ peak also expected for a hexagonal structure was observed, at higher temperatures in the melt.) Two Bragg peaks were observed at higher q that are due to smectic layering. This is illustrated in Figure 4, which presents scattering data obtained with a shorter sample-to-detector distance than in Figure 3. The smectic period is found to be $d_s = 35.0 \pm 0.3$ Å.

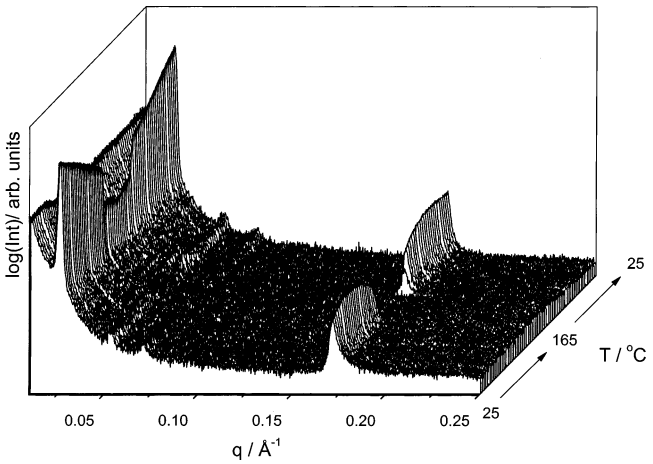

Figure 5. SAXS data obtained for Z11 during a heat/cool ramp from 25 to 125 °C and back to 25 °C at 3 °C/min.

The smectic phase melts at $T = 101 \pm 2$ °C, in good agreement with the value from DSC. The first-order smectic reflection was observed to orient under large-amplitude oscillatory shear, as discussed elsewhere.[23]

Figure 5 contains SAXS data for Z11, confirming that the disordering (and subsequent reordering) of the hexagonal block copolymer structure occurs at the smectic−isotropic transition. The ordering on the two length scales appears to be correlated in our side-group liquid-crystal block copolymer. Hammond et al. have reported that the block copolymer ODT and clearing point are coincident if the polymer molar mass is low and/or the LC block volume fraction is low, whereas for polymers with a higher molar mass and/or LC volume fraction, the ODT can occur at a higher temperature than the clearing point because of the increased degree of segregation.[18,20] Yamada et al. found that the smectic−isotropic transition temperature increased with molar mass for their SGLC−BCPs up to a molecular weight, beyond which it became nearly constant.[16] However, they did not determine the ODT for their polymers. Ikkala et al.[21] also observed the persistence of block copolymer ordering above the liquid-crystal phase transition in their block copolymer−hydrogen-bonded amphiphile complexes.

The ODT of our block copolymers be precisely located from discontinuities in the intensity and width of the SAXS peaks. Figure 6 shows the inverse intensity and peak position (obtained from fits using a Gaussian function with a sloping background) of the first-order reflection. The data are presented against inverse temperature, consistent with the ODT determination for nonmesogenic block copolymers,[3] this presentation being motivated by Leibler's random phase approximation theory for the structure factor.[26] Anthamatten and Hammond have located the ODT of their side-group liquid-crystal block copolymers in a similar fashion.[20] Figure 6 shows a sharp discontinuity in (inverse) intensity that defines the ODT at 101.5 °C. The intensity shows little hysteresis associated with a heat−cool cycle. Interestingly, although the peak position q^* is continuous across the ODT, there is a change in gradient. Below the ODT, the decrease in q^* with increasing temperature is consistent with thermal expansion. Above the ODT, q^* is associated with the broad correlation hole peak, the position of which increases with temperature, possibly due to changes in backbone conformation across the smectic−isotropic transition (coincident with the ODT). A change

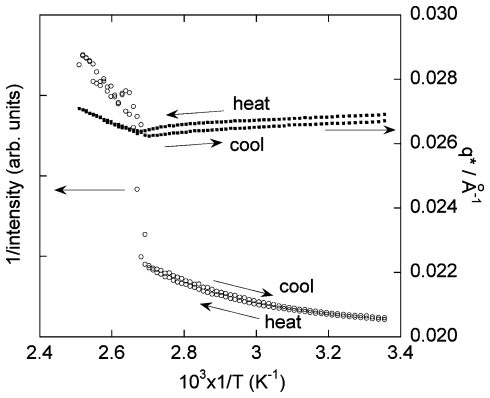

Figure 6. Analysis of variation in inverse intensity and position of the maximum of the first SAXS peak in the data presented in Figure 5. The data are plotted against inverse temperature, consistent with the presentation of small-angle scattering data for nonmesogenic block copolymers.

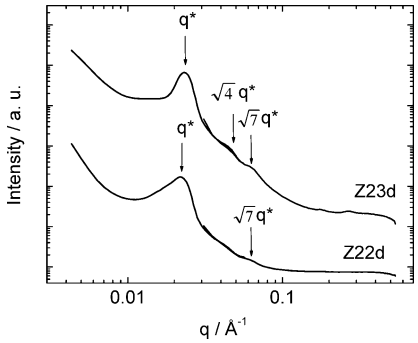

Figure 7. SANS intensity profiles obtained (at the ILL, Grenoble) for Z22d and Z23d at $T = 80$ °C. The curve for Z22d has been offset by a factor of 100 for clarity. The arrows indicate the positions of small-angle reflections observed. Wide-angle reflections can also be noted for Z23d.

in gradient of q^* across the ODT (although not necessarily a change in sign of gradient) has been reported previously for nonmesogenic block copolymers.[3] The intensity changes discontinuously at exactly the same temperature as the disappearance of the smectic peak as confirmed by Gaussian peak fitting and also apparent in Figure 5. A small degree of hysteresis can be noted for q^* (perhaps associated with a change in backbone conformation after melting), although the intensity is very similar on heating and cooling.

SANS was performed on the two samples with d_8-polystyrene blocks with the aim of examining chain configuration and the orientation of the backbone with respect to mesogens on samples aligned in a magnetic field. The smectic layer structures for these samples produced very weak Bragg peaks, although this may be due to the decrease in intensity at the detector with increasing angle. Figure 7 shows data obtained (at the ILL) in the absence of a magnetic field; similar data were obtained (at ISIS) in a magnetic field. For Z23d a weak peak at $q = 0.18$ Å^{-1} is apparent, corresponding to the usual 35 Å smectic layer spacing (together with an additional reflection at $q = 0.27$ Å^{-1} that corresponds to $d = 23$ Å, the origin of this latter peak being unclear at present). However, for Z22d this peak was absent. In the small-angle region, Z23d shows a sharp reflection at $q^* = 0.023$ Å^{-1}, with higher orders at $\sqrt{4}q^*$ and $\sqrt{7}q^*$, indicating a hexagonal structure, which must comprise cylinders of polystyrene, when the composition is considered. The expected peak at $\sqrt{3}q^*$ may contribute to the wide second-order peak. Alternatively, it may be absent, either due to the presence of a minimum in the form factor of the cylinders or due to distortion of the hexagonal lattice. For sample Z22d, the structure is also probably hexagonal-packed cylinders, given the presence of two reflections at q^* and $\sqrt{7}q^*$ and considering the composition of the copolymer. In this case, the cylinders comprise the mesogen-bearing block in a matrix of polystyrene. The first-order peak is extended toward low q. We note that the apparently lower value of q^* for Z22d in Figure 8 results from this extension of the peak to low q (see Figure 7).

Because of the presence of weak or absent smectic layer peaks, attempts to investigate the magnetic alignment of the mesogens were frustrated. However, orientation of the microphase-separated structure was observed. The procedure we employed, whereby the sample is slowly cooled in the presence of a magnetic field from the isotropic phase into the liquid-crystal phase, has previously been shown to lead to significant backbone anisotropy in side-chain liquid-crystal homopolymers.[27−29] In the liquid-crystal block copolymer Z22d, a magnetic field induces orientation of the LC cylinders in the polystyrene matrix in the smectic phase, as shown by comparing the SANS patterns in Figure 8a,b. No anisotropy is observed at 130 °C in the isotropic phase of the mesogens (thus confirming that no shear-induced alignment of the PS cylinders occurred). However, there is pronounced anisotropy at 70 °C after cooling through the smectic phase (to a point below the polystyrene glass transition). The arcs of scattering around the equator point to orientation of the cylinders in the vertical direction. In contrast, there is no evidence for magnetic orientation in Z23d, which has a structure inverse to that of Z22d, i.e., PS cylinders in an LC matrix. It may seem surprising that orientation is observed for the case of LC cylinders in a glassy PS matrix (and not vice versa). However, it has to be considered that the self-assembly on slow cooling is a cooperative process in which the glass transition and smectic−isotropic phase transition occur very close to one another. Orientation must occur in the state in which PS is still molten. The LC cylinders are anisotropic objects containing a small number of smectic layers of mesogens that are susceptible to orientation. This orientation may be trapped upon vitrification of the polystyrene. In contrast, in the inverse structure the PS cylinders in the LC matrix may act as sites for the anchoring of defects, thus hindering macroscopic alignment. A similar effect is observed when spherical colloidal particles are added to a liquid-crystal fluid.[30,31] However, this argument is not supported by prior work that indicates that samples containing polystyrene cylinders in an LC matrix can be aligned by flow.[4,12] It is possible that the dynamics of orientation in a magnetic field differ from those under flow or that the viscosity of the smectic phase plays a role. This issue clearly requires further investigation. Although we could not probe liquid-crystal layer alignment in Z22d, we are able to infer it from the observed orientation of the liquid-crystalline cylinders, which must result from alignment of the mesogens along the magnetic field direction (horizontal). This would produce smectic layers parallel to cylinders, which align perpendicular to the field. This is illustrated in Figure 9, which contains schematics of the aligned cylinder structure in Z22d and the unoriented structure of Z23d. A homogeneous

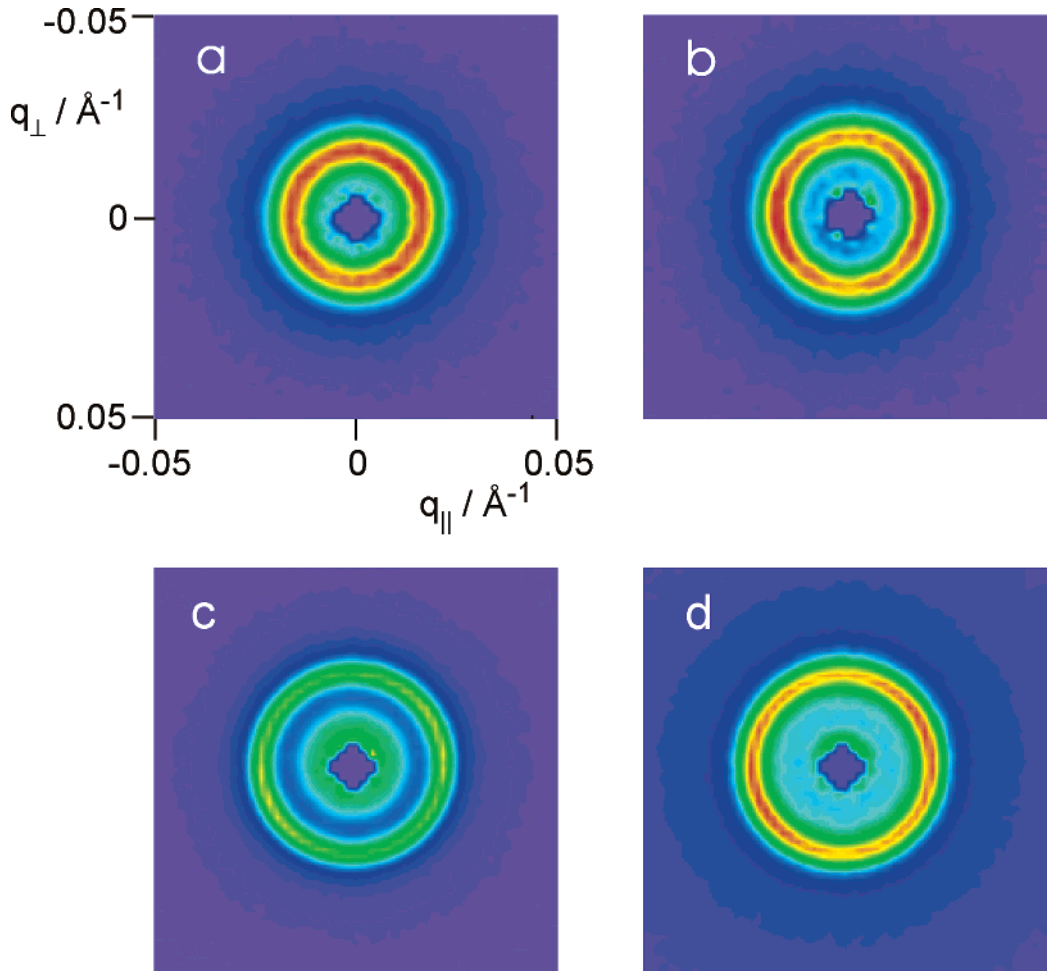

Figure 8. SANS patterns obtained in the presence of a magnetic field: (a) Z22d in the isotropic phase at 130 °C, (b) Z22d in the vitrified smectic phase at 70 °C, (c) Z23d in the isotropic phase at 130 °C, and (d) Z23d in the vitrified smectic phase at 70 °C. For each polymer, the two pairs of patterns are shown on the same linear intensity scale (maximum intensity = 130 arbitrary units for Z22d and maximum intensity = 400 arbitrary units for Z23d) to facilitate comparison. The magnetic field direction was horizontal.

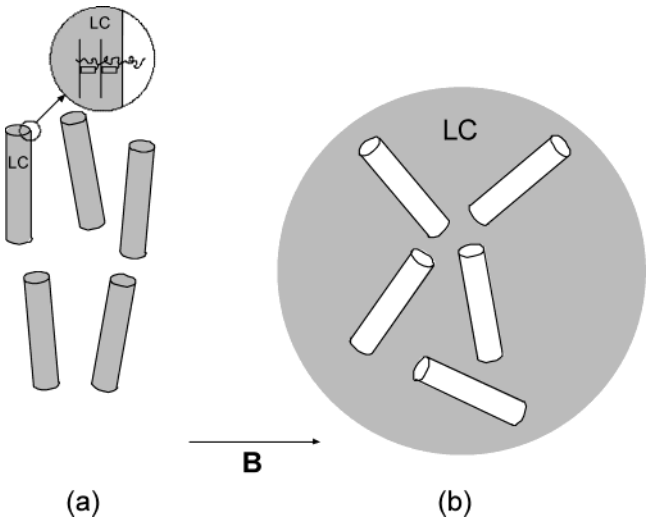

Figure 9. Schematic showing (a) aligned structure of LC cylinders in an PS matrix (as in Z22d) and (b) unoriented structure of PS cylinders in an LC matrix (as in Z23d). The magnetic field direction is indicated.

orientation (mesogens parallel to cylinder walls) has previously been reported for cylinder-forming SGLC−BCPs.[11,12] In our sample, the decoupling of mesogen from the backbone due to the long spacer may enable mesogens to align perpendicular to the cylinders. This is consistent with reports on a lamellar SGLC−BCP with a long decyl spacer for which a parallel layer alignment was observed, in contrast to the perpendicular layer orientation in a sample with a hexyl spacer.[4]

3.3. Thin Film Nanostructures. In many potential applications, for example as liquid-crystal alignment substrates, side-group liquid-crystal block copolymers will be present in the form of thin films. We therefore examined the thin film structure of selected copolymers, using a combination of atomic force microscopy to probe the morphology at the surface and specular X-ray reflectivity to determine the ordering perpendicular to the substrate. In the following, we focus on sample Z11 since the bulk morphology of this was determined unambiguously; however, AFM and X-ray reflectivity were also performed for Z22d. Figure 10 shows a phase contrast image of the polymer surface, containing prominent domains of stripelike patterns coexisting with domains of local hexagonal ordering (particularly evident in the center right portion of the image). The combination of these two features supports the presence of a hexagonal-packed cylinder phase, two projections of which are imaged at the surface. The stripe domains correspond to cylinders viewed “edge on”, and the regions of circular domains correspond to “end-on” cylinders. Coexisting parallel and perpendicular cylinders were previously observed by AFM for a nonme-

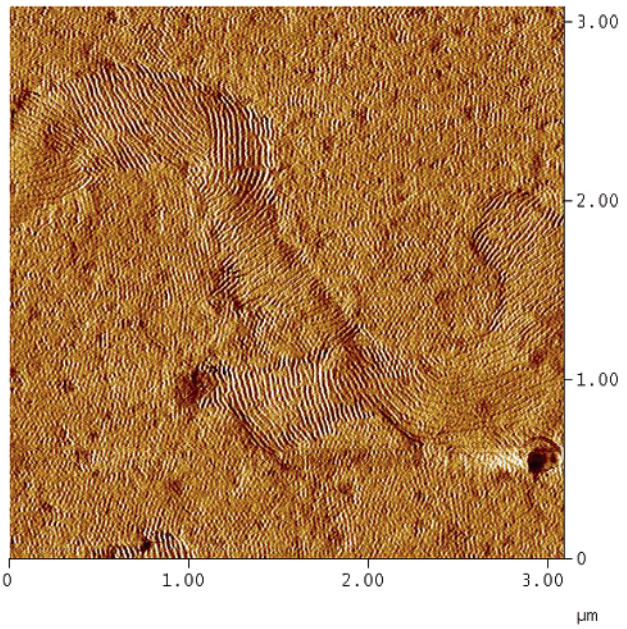

Figure 10. AFM image (phase contrast mode) obtained at room temperature for Z11 annealed overnight at 130 °C.

sogenic PS−PB−PS triblock.[32] It is interesting that this mixed morphology persists even after annealing overnight at high temperature (130 °C)—it would be expected on surface energy grounds that the lower surface energy component would preferentially segregate to the polymer−air interface. It may be that we are imaging (in phase contrast mode) buried "hard" cylinders through a thin top layer. Alternatively, there may be PS cylinders at the surface due to reduced kinetics of microstructure rearrangement for the confined structure, an effect already noted for PS-based block copolymers with a nonmesogenic block.[33] It is not possible to differentiate these two possibilities at present. We note that the structure in very thin films probed by AFM does not necessarily correspond to the bulk structure, although the bulk limit is recovered for sufficiently thick films.[34] Ellipsometry (phase-modulated spectroscopic ellipsometer, Beaglehole Instruments) was employed to measure the thickness of the film on silica studied by AFM, which was found to be 933 ± 7 Å, corresponding to just over four layers, i.e., definitely not the bulk limit.

To probe the structure perpendicular to the substrate, the same film was studied by X-ray reflectivity. Figure 11 shows profiles obtained at four temperatures. The data at $T = 120$ °C and $T = 105$ °C show weak fringes, resulting from interference between X-rays scattered from the polymer−substrate and polymer−air interfaces, where the largest step changes in electron density occur. There is no evidence for layer order, as indicated by the absence of Bragg reflections. In contrast, a strong Bragg peak is observed in the profile at 85 °C with a peak that corresponds to a layer spacing $d = 33.8$ Å (see details of modeling below) close to the bulk layer spacing. This indicates the presence of smectic layers aligned parallel to the substrate. The occurrence of the isotropic−smectic transition between 105 and 85 °C is consistent with SAXS and DSC on the bulk sample. Interestingly, there is no evidence for Bragg peaks from the block copolymer microstructure at lower q. It has to be noted, however, that the bulk $q^* = 0.0285$ Å^{-1} would fall below the critical q for total external reflection, which is observed at $q = 0.03$ Å^{-1}, close to the value expected for Si or SiO_2.[35] Therefore, X-ray reflectivity does not provide information on the extent to which the polystyrene cylinders are lying parallel or perpendicular to the substrate (AFM on the same sample suggests mixed alignment; Figure 10).

To obtain quantitative information about the smectic layering from the reflectivity profiles, they were modeled using an iterative matrix solution of the Fresnel equations for a multilayer system.[36] The corresponding fits are shown in Figure 12 and correspond closely to the data. The films were represented by a SiO_2 layer on top of the Si, followed by a number of slabs corresponding to smectic layers. A total of 30 layers was found to fit the data well. It was necessary to divide each layer into two sublayers with different electron densities, which presumably correspond to the mesogenic core (thick, high electron density region) and spacer and backbone

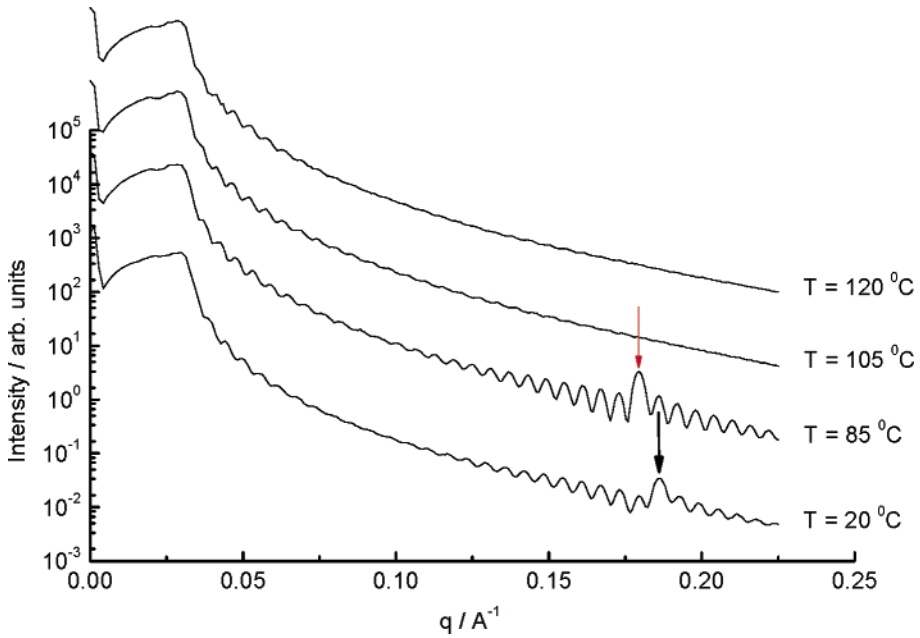

Figure 11. X-ray reflectivity profiles for Z11 obtained at the temperatures indicated. The red arrow indicates the position of the smectic layer peak at 85 °C, and the black arrow indicates that at 20 °C.

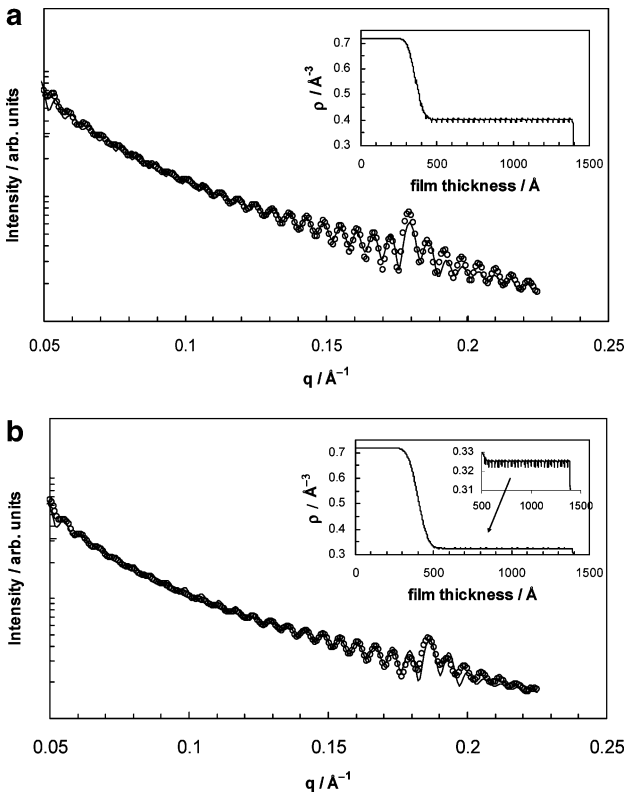

Figure 12. Fits to the X-ray reflectivity profiles for Z11 at (a) 85 and (b) 20 °C. The solid lines are the reflectivity profiles calculated using the electron density profiles shown in the insets. The points are the measured data. Fit parameters are listed in Table 5.

Table 5. Parameters in Multilayer Model Used To Fit X-ray Reflectivity Data

layer	ρ/e Å^{-3}	t/Å	σ/Å
20 °C			
SiO_2	0.714	125	45
1st sublayer	0.325	29.8	3.9
2nd sublayer	0.321	3.5	0
85 °C			
SiO_2	0.714	125	45
1st sublayer	0.404	31.8	4.4
2nd sublayer	0.385	2.8	0

(thin, low electron density region). A Gaussian interfacial roughness parameter, σ, was an additional model parameter for the SiO_2 layer and the dense smectic sublayers. The parameters obtained from the fits are listed in Table 5. The total film thickness at 20 °C from the model is 999.9 Å. Taking into account thermal expansion, this is in good agreement with the value obtained by ellipsometry at room temperature. On reducing the temperature below the glass transition temperature (of the polystyrene block), the X-ray reflectivity profile is similar, although with a pronounced shift in Bragg peak position, indicating a smaller layer spacing d = 33.3 Å. The electron density of both sublayers is also reduced at low temperature (as is the difference in electron density). This suggests that vitrification in thin films leads to less well-defined smectic layers. The fact that X-ray reflectivity reveals a Bragg peak arising from parallel smectic layers does not imply that they are all parallel. Any fraction oriented perpendicular to the surface will not contribute to the specular signal. Wu et al. have previously reported a mixed orientation with planar and homeotropic orientation of mesogens in an islanded film formed by a SGLC−BCP, depending on the local film thickness.[37] Sentanac et al. have shown that the orientation of mesogens with respect to block copolymer microdomains (lamellar in their case) can be influenced by surface fields in thin films.[38] They observed smectic layers parallel to the lamellae in thin films, in contrast to a perpendicular orientation in bulk. In the absence of off-specular X-ray reflectivity data, we are not able to assess the relative extent of planar vs homeotropic mesogenic layer alignment.

4. Summary

Hierarchical ordering was observed in several side-group liquid-crystal block copolymers. The copolymers were synthesized via atom transfer radical polymerization and comprise a nonmesogenic polystyrene block and a poly(methyl methacrylate)-based block with pendant biphenyl chiral ester moieties attached to the backbone by a dodecyloxy spacer. SAXS and WAXS were used to probe microphase separation of the block copolymer and liquid-crystal ordering, respectively. All samples exhibit a smectic phase. The smectic−isotropic phase transition temperature and enthalpy were determined by DSC. DSC also located two glass transition temperatures—for the polystyrene block at around 100 °C (close to the smectic−isotropic transition) and for the mesogen-bearing block (at 5−10 °C). Hexagonal-packed cylinder morphologies were observed, comprising either glassy polystyrene cylinders in a liquid crystal matrix or LC cylinders in a polystyrene matrix.

Small-angle neutron scattering was used to probe orientation in a magnetic field for the case of two polymers containing a perdeuterated polystyrene block. The samples were slow cooled from the isotropic phase below the isotropic−smectic transition (polystyrene glass transition) in the presence of a magnetic field. Orientation was observed for the sample comprising LC cylinders in a polystyrene matrix, but not the inverse structure. It is suggested that orientation occurs in the former case in the molten state where the anisotropic mesogenic rods are susceptible to magnetic orientation. In contrast, the polystyrene rods in the LC matrix may act as nucleation sites for defects, hindering long-range alignment. Alternatively, the high viscosity of the smectic layers may influence the extent and kinetics of alignment.

The morphology in thin films was probed by AFM and X-ray reflectivity. For a sample comprising PS cylinders in an LC matrix, AFM revealed a mixed orientation at the polymer−air surface in a thin film after annealing. Cylinders were observed oriented both parallel and perpendicular to the substrate. X-ray reflectivity on the same sample revealed smectic layering (below the smectic−isotropic transition) with a similar layer spacing to that in bulk. The presence of some smectic layers aligned parallel to the substrate was thus confirmed.

Taken together, the combination of techniques applied to study the interplay between liquid-crystal and block copolymer ordering in bulk and in thin films provided unprecedented insight into these fascinating nanostructured materials.

Acknowledgment. This work was supported by EPSRC, UK (Grant GR/N12190 to I.W.H.). We thank Imtiyaz Ansari for technical assistance and Tetyana Mykhaylyk for the AFM image (Figure 10). We are grateful to ISIS for the provision of beamtime on LOQ

(ref 14489) and to Steve King for assistance with the experiments. Beamtime at the Institute Laue Langevin was on instrument D22 (experiment 9-11-996).

References and Notes

(1) *Side Chain Liquid Crystal Polymers*; McCardle, C. B., Ed.; Blackie: London, 1989.
(2) Hsu, C.-S. *Prog. Polym. Sci.* **1997**, *22*, 829.
(3) Hamley, I. W. *The Physics of Block Copolymers*; Oxford University Press: Oxford, 1998.
(4) Anthamatten, M.; Zhang, W. Y.; Hammond, P. T. *Macromolecules* **1999**, *32*, 4838.
(5) Fischer, H.; Poser, S.; Arnold, M. *Liq. Cryst.* **1995**, *18*, 503.
(6) Anthamatten, M.; Wu, J.-S.; Hammond, P. T. *Macromolecules* **2001**, *34*, 8574.
(7) Anthamatten, M.; Hammond, P. T. *J. Polym. Sci., Part B: Polym. Phys.* **2001**, *39*, 2671.
(8) Walther, M.; Finkelmann, H. *Prog. Polym. Sci.* **1996**, *21*, 951.
(9) Hamley, I. W. *Adv. Polym. Sci.* **1999**, *148*, 113.
(10) Fischer, H.; Poser, S.; Arnold, M.; Frank, W. *Macromolecules* **1994**, *27*, 7133.
(11) Mao, G.; Wang, J.; Clingman, S. R.; Ober, C. K.; Chen, J. T.; Thomas, E. L. *Macromolecules* **1997**, *30*, 2556.
(12) Osuji, C.; Zhang, Y.; Mao, G.; Ober, C. K.; Thomas, E. L. *Macromolecules* **1999**, *32*, 7703.
(13) Adams, J.; Gronski, W. In *Liquid Crystal Polymers*; Wein, D. A., Ober, C. K., Eds.; American Chemical Society: Washington, DC, 1990; Vol. 433.
(14) Yamada, M.; Iguchi, T.; Hirao, A.; Nakahama, S.; Watanabe, J. *Macromolecules* **1995**, *28*, 50.
(15) Zheng, W.-Y.; Albalak, R. J.; Hammond, P. T. *Macromolecules* **1998**, *31*, 2686.
(16) Yamada, M.; Itoh, T.; Nakagawa, R.; Hirao, A.; Nakahama, S.; Watanabe, J. *Macromolecules* **1999**, *32*, 282.
(17) Fischer, H.; Poser, S. *Acta Polym.* **1996**, *47*, 413.
(18) Zheng, W. Y.; Hammond, P. T. *Macromolecules* **1998**, *31*, 711.
(19) Sänger, J.; Gronski, W.; Maas, S.; Stühn, V.; Heck, B. *Macromolecules* **1997**, *30*, 6783.
(20) Anthamatten, M.; Hammond, P. T. *Macromolecules* **1999**, *32*, 8066.
(21) Ruokolainen, J.; Mäkinen, R.; Torkkeli, M.; Mäkelä, T.; Serimaa, R.; ten Brinke, G.; Ikkala, O. *Science* **1998**, *280*, 557.
(22) Polushkin, E.; van Ekenstein, G. A.; Dolbnya, I.; Bras, W.; Ikkala, O.; ten Brinke, G. *Macromolecules* **2003**, *36*, 1421.
(23) Ansari, I. A.; Castelletto, V.; Mykhaylyk, T.; Hamley, I. W.; Lu, Z. B.; Itoh, T.; Imrie, C. T. *Macromolecules* **2003**, *36*, 8898.
(24) Lu, Z. B.; Imrie, C. T.; Ansari, I. A.; Castelletto, V.; Hamley, I. W. Manuscript in preparation.
(25) Hamley, I. W.; Pople, J. A.; Gleeson, A. J.; Komanschek, B. U.; Towns-Andrews, E. *J. Appl. Crystallogr.* **1998**, *31*, 881.
(26) Leibler, L. *Macromolecules* **1980**, *13*, 1602.
(27) Davidson, P.; Noirez, L.; Cotton, J. P.; Keller, P. *Liq. Cryst.* **1991**, *10*, 111.
(28) Noirez, L.; Davidson, P.; Scwarz, W.; Pépy, G. *Liq. Cryst.* **1994**, *16*, 1081.
(29) Noirez, L.; Keller, P.; Cotton, J. P. *Liq. Cryst.* **1995**, *18*, 129.
(30) Meeker, S. P.; Poon, W. C. K.; Crain, J.; Terentjev, E. M. *Phys. Rev. E* **2000**, *61*, 6083.
(31) Guzmán, O.; Kim, E. B.; Grollau, S.; Abbott, N. L.; de Pablo, J. J. *Phys. Rev. Lett.* **2003**, *91*, 235507.
(32) van Dijk, M. A.; van den Berg, R. *Macromolecules* **1995**, *28*, 6773.
(33) Kim, G.; Libera, M. *Macromolecules* **1998**, *31*, 2670.
(34) Knoll, A.; Horvat, A.; Lyakhova, K. S.; Krausch, G.; Sevink, G. J. A.; Zvelindovsky, A. V.; Magerle, R. *Phys. Rev. Lett.* **2002**, *89*, 035501.
(35) Russell, T. P. *Mater. Sci. Rep.* **1990**, *5*, 171.
(36) Hamley, I. W.; Pedersen, J. S. *J. Appl. Crystallogr.* **1994**, *27*, 29.
(37) Wu, J.-S.; Fasolka, M. J.; Hammond, P. T. *Macromolecules* **2000**, *33*, 1108.
(38) Sentenac, D.; Demirel, A. L.; Lub, J.; de Jeu, W. H. *Macromolecules* **1999**, *32*, 3235.

MA0498619